Loss and Heat Computations of Damper Bars in Large Tubular Hydro-Generator

Zhen-nan Fan[1,2], Li Han[1], Guang-hou Zhou[1,3], Xiao-quan Hou[3], Yi-gang Liao[3]

[1] School of Electrical Engineering, Chongqing University, Chongqing, 400044, P. R. China

[2] Sichuan Electric Vocational and Technical College, Chengdu, 610072, P. R. China

[3] Dongfang Electrical Machinery Company Limited, Deyang, 618000, P. R. China

***Abstract*-To research the loss and heat of damper bars thoroughly, a 2D electromagnetic field FE model of tubular hydro-generator and a 3D temperature field FE model of the rotor are built up respectively. The factors such as rotor motion and nonlinearity of the time-varying electromagnetic field, the anisotropic heat conduction of the rotor core lamination and different heat dissipation conditions on the windward and lee side of the poles are considered. Furthermore, according to the different operating conditions, different rotor structures and materials, compositive calculations about the losses and temperatures of the damper bars of a 36MW generator are carried out, and the data are compared with the test. The results show that the computation precision is satisfied and the generator design is reasonable.**

I. INTRODUCTION

DAMPER winding is one of the key components of hydro-generator and plays an important role for the safety and stability of generator and power system. The tubular hydro-generator is a good type of hydro-generators which is suitable for exploiting and utilizing the hydraulic resources with low water head and large flowrate. Compared with the axial flowing hydro-generator with the same capability, tubular hydro-generator can economize the project investment 10-25% and increase 3-5% of the power every year, it has then been applied widely at the hydropower stations whose water head is lower than 20m [1]. However, the electromagnetic and cooling designs of the tubular hydro-generators are more difficult because of its limited inner space and then the more possibility of over heat. In recent years, heavy broken-down failures of damper bars in some large tubular hydro-generators operating at different power stations occurred due to the high temperature at the rated load [2][3]. To improve the generator design and avoid these serious failures, the amount and distribution of losses and temperatures within the rotor of the tubular hydro-generators need to be computed more accurately.

Copper losses of field winding and damper bars, as well as iron core losses of rotor lamination, exist within the rotor. For the complex rotor structure of hydro-generator, all of these losses are difficult to compute accurately except the loss of field winding. When the movement of rotor is considered, the heat dissipation condition of the rotor components are more difficult to confirm precisely. Though FE method has been widely used in the temperature field calculation of generators [4-11], the papers about FE calculation of damper bars losses and temperatures in large tubular hydro-generators are scarce.

In [7], a 3D isoparametic element method was used to research the influence about the different heat dissipation condition of the pole windward and lee side to the temperature field in the middle and end region of the rotor, and the influence about the additional loss to the rotor temperature field. In [8] and [9], the calculations of rotor 3D temperature field were combined with the ventilation network of a large hydro-generator and the temperature distribution of the rotor was obtained. However, their rotor losses were calculated by the analytical formulae and the factors of rotor motion and the eddy current in damper bars were not considered in [7], [8] and [9]. In [10], no load airgap magnetic field of a salient pole synchronous generator was calculated by the steady magnetic field FE method, the analytical formula was also used to deal with the rotor losses, but the factors such as the time-varying influence of electromagnetic field and the damper bars eddy current losses at the rated load were not considered yet. In [11], time-stepping FE analysis was used to deal with the rotor motion, and the normal and broken damper bar currents were calculated, but the losses and temperatures of the damper bars were not concerned. To analyze the damper bar broken-down failure of tubular hydro-generator at *Feilaixia* power station, the calculations of 2D transient electromagnetic field and 3D temperature field were mentioned in [3], but the relative algorithm or formula was not given.

To research the loss and heat thoroughly and avoid the broken-down failure of damper bars in large tubular hydro-generators, a 2D electromagnetic field FE model and a 3D temperature field FE model are established respectively in this paper. The important factors, such as rotor motion and nonlinearity of the time-varying electromagnetic field, the anisotropic heat conduction of the rotor core lamination and different heat dissipation conditions on the windward and lee side of the poles, are considered. Furthermore, according to the different operating conditions, different rotor structures and materials, compositive calculations about the losses and temperatures of the damper bars of a 36MW tubular hydro-generator at *Tongzihao* power station are carried out. The

Corresponding author: Li Han (hanli@cqu.edu.cn)

design data, which are listed in TABLE I, are compared with other large tubular hydro-generators at *Linjintan* and *Feilaixia* power stations. And the results are compared with the test.

II. Calculation Models

A. Boundary value problem of moving electromagnetic field

According to the periodicity of magnetic field distribution, the domain within a couple of poles is chosen as the problem region of electromagnetic field solving, which includes 10 123 elements and 27 683 nodes, as shown in Fig. 1.

The governing equation of nonlinear time-varying electro-magnetic field is [13]

$$\nabla\times(\nu\nabla\times\mathbf{A})+\sigma\left[\frac{\partial\mathbf{A}}{\partial t}-\mathbf{V}\times(\nabla\times\mathbf{A})\right]=\mathbf{J_S} \tag{1}$$

where $\mathbf{A}$ is vector magnetic potential, $\mathbf{J_s}$ is source current density, ν is reluctivity, $\mathbf{V}$ is velocity and σ is conductivity.

In the 2D field, the source current density and vector potential have only z-axis component respectively, and the speed has only x-axis component. By coulomb norm $\nabla\cdot\mathbf{A}=0$ and the boundary condition of the problem region, the boundary value problem of nonlinear time-varying moving electromagnetic field for the generator is then obtained:

$$\begin{cases}\dfrac{\partial}{\partial x}(\nu\dfrac{\partial A_z}{\partial x})+\dfrac{\partial}{\partial y}(\nu\dfrac{\partial A_z}{\partial y})=-J_{sz}+\sigma\dfrac{\partial A_z}{\partial t}+V_x\sigma\dfrac{\partial A_z}{\partial x}\\ A_z\big|_{AB}=A_z\big|_{CD}=0\\ A_z\big|_{AC}=A_z\big|_{BD}.\end{cases} \tag{2}$$

B. Loss calculation of damper bars

By FE post-processing, the eddy current density, the eddy current and its loss per element in the damper bar are obtained:

TABLE I
Comparison of the Basic Data of the Generators

	Tongzihao generator	*Linjintan* generator	*Feilaixia* generator
Rated power (MW)	36	30	35
Rated voltage (kV)	10.5	10.5	10.5
Rated current (A)	2 151	1 736	2 144
Power factor	0.92	0.95	0.9
Rated field current (A)	857	943	1 079
Number of magnetic poles	72	76	72
Number of stator slots	324	342	324
Number of damper bars per pole	4	4	3
Damper bar condition	Good	Broken	Broken

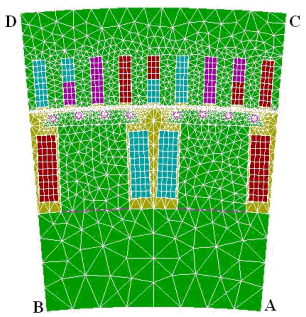

Fig. 1 The problem region and meshes of 2D electromagnetic field

$$J=-\sigma_b\frac{\partial A_z}{\partial t}, \tag{3}$$

$$I_e=\iint_{\Delta_e}J dxdy, \tag{4}$$

and

$$p_e=I_e^2\frac{L_b}{\sigma_b\Delta_e} \tag{5}$$

where σ_b is the conductivity of damper bar, L_b is the length of damper bar, Δ_e is the area of an element in the damper bar region.

The eddy current loss in one damper bar can then be calculated by

$$p_{db}=\sum_{e=1}^{E_b}p_e \tag{6}$$

where E_b is the number of FE elements in one damper bar.

C. Loss calculation of rotor iron core

FE method is used to analyze the no load operation of the generator. After the average flux density B_δ in the airgap is computed, the iron losses can be calculated as following.

The no load additional iron core loss on the surface of pole shoe is induced by the tooth harmonics of uneven airgap reluctance and is formulated as [14]:

$$p_{Fep0}=k_0\left[\frac{(K_{\delta1}-1)B_\delta t_1}{1000}\right]^2\left[\frac{Zn_N}{10000}\right]^{1.5}\frac{2pA_p}{1000}\times10^{-7} \tag{7}$$

where k_0 is the coefficient related with the magnetic characteristic and the thickness of rotor core lamination, $K_{\delta1}$ is the airgap coefficient of the stator tooth, t_1 is the stator tooth pitch, Z is the number of stator slots, n_N is the rated speed of generator, p is the number of pole pairs and A_p is the area on the surface of the pole shoe.

The rated load additional iron core loss on the surface of pole shoe, induced by the stator tooth harmonic magnetic field, is then obtained according to (7):

$$p_{2tk}=k'\left[X^*_{ad}\frac{2p}{Z(K_{\delta1}-1)}\right]^2p_{Fep0} \tag{8}$$

Where k' is the coefficient related with the airgap shape, X^*_{ad} is the per-unit value of the d-axis armature reactance.

Another rated load additional iron core loss on the surface of pole shoe, induced by the phase-belt harmonic emf of the stator winding, is given by [14][15]:

$$p_{2vk}=\sum k_0'(B_{vb}2\tau_v)^2f_v^{1.5}k_{rv}^2A_p \tag{9}$$

where v=5,7,11,…, k'_0 and k_{rv} are the coefficients related with the core material respectively, B_{vb} is the amplitude of the v^{th} phase-belt harmonic flux density, τ_v and f_v are the pole pitch and the frequency of the v^{th} harmonic field respectively.

By (7), (8) and (9), all core iron losses of the generator rotor are then obtained:

$$p_{iron}=p_{Fep0}+p_{2tk}+p_{2vk} \tag{10}$$

D. Treatment of the rotor motion

Relative movement of the rotor results in the change of FE

mesh subdivision. It is necessary to treat with the rotor motion carefully to ensure the convergence and precision of time-stepping FE solution. The rotating airgap technique is used and a thin transitional element layer within the middle of the airgap is defined, as shown in Fig. 2. When the rotor moves to a new position in the time-stepping FE calculation, the elements in the rotating airgap are remeshd, but the others remain unchanged.

E. Boundary value problem of rotor 3D temperature field

Because of the symmetric structures of the rotor pole and its ventilation system , the distribution of rotor temperature field is mirror symmetric on the both sides of the rotor shaft middle profile. Therefore, an half axial section of the rotor, which consists of rotor core, damper winding, field winding and its bracket, insulation, et al, are selected as the problem region for the 3D temperature field solving, and the region includes 23 8670 elements and 13 1967 nodes.

Taking account of the anisotropic heat conduction condition of the rotor core, the boundary value problem of 3D steady temperature field can be expressed as follows:

$$\begin{cases} \dfrac{\partial}{\partial x}(\lambda_x \dfrac{\partial T}{\partial x}) + \dfrac{\partial}{\partial y}(\lambda_y \dfrac{\partial T}{\partial y}) + \dfrac{\partial}{\partial z}(\lambda_z \dfrac{\partial T}{\partial z}) = -q_V \\ \lambda \dfrac{\partial T}{\partial n}\Big|_{S_2} = 0 \\ \lambda \dfrac{\partial T}{\partial n}\Big|_{S_3} = -\alpha(T - T_f) \end{cases} \tag{11}$$

where T is temperature, λ_x, λ_y and λ_z are heat conductivity on each direction, q_v is the heat source density which is obtained by losses calculation mentioned above, S_2 are the rotor middle profile and the interface between rotor core and rim related with the thermal insulation boundary condition, S_3 are the outside surfaces of the rotor related with the heat dissipation boundary condition, α is the heat dissipation coefficient of S_3 and T_f is the environmental air temperature. The problem region and boundary conditions are illustrated in Fig. 3.

The heat dissipation coefficients on the end and top surfaces of the pole shoe and field winding are as following respectively [14]:

$$\alpha = \frac{1 + 0.1\tau}{450} \tag{12}$$

$$\alpha'' = K\alpha' \tag{13}$$

where τ is the pole pitch, K and α' are the coefficients related with the generator structure respectively.

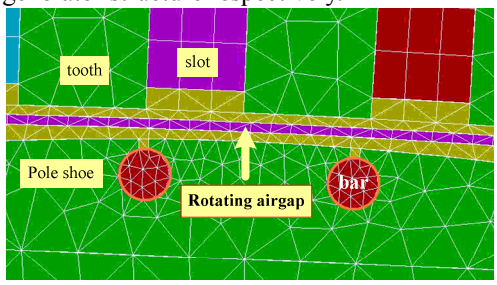

Fig. 2 The rotating airgap and elements of sub-region

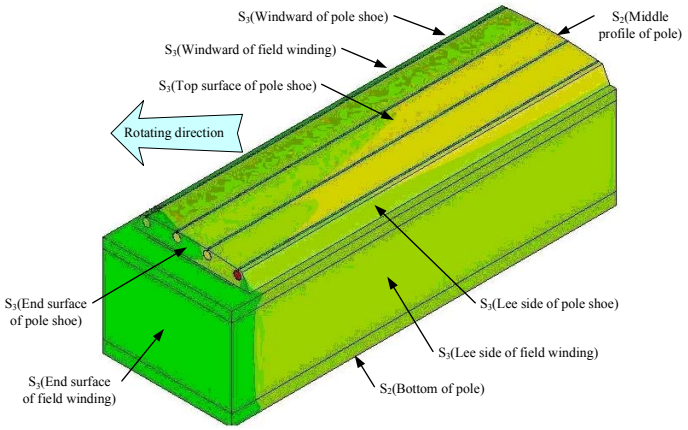

Fig. 3 The problem region and boundary conditions of 3D temperature field

Considering the better cooling condition on the windward, the heat dissipation coefficients of the pole shoe and field winding are enlarged 20% respectively. On the other hand, the heat dissipation coefficients on the lee side of the pole shoe and field winding are reduced 20% respectively due to their worse cooling condition.

III. COMPUTATION RESULTS AND DISCUSSIONS

Based on the models established above, the compositive computations of 2D electromagnetic field and 3D temperature field of the 36MW tubular hydro-generator at *Tongzihao* power station are carried out. There are 4 damper bars on each pole shoe. For easy discussion of the computing results, the damper bar on the lee side is numbered 1th and the damper bar on the windward is numbered 4th.

A. The influence of operating conditions

Fig. 4 gives the electromagnetic field, the eddy current and the temperature distributions on the no load and rated load of the generator respectively. TABLE II gives the losses and temperatures of the damper bars with 3 different operating conditions, no load, symmetric rated load, asymmetric rated load with 12% negative sequence current (IEC test standard).

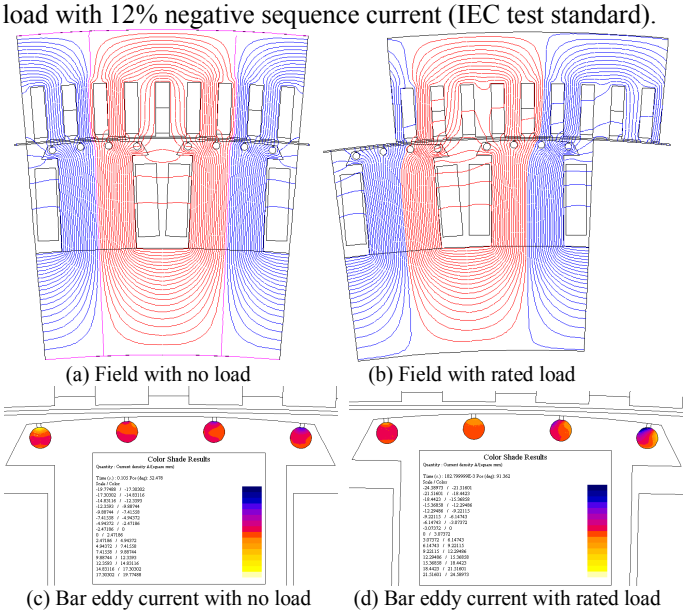

(a) Field with no load (b) Field with rated load

(c) Bar eddy current with no load (d) Bar eddy current with rated load

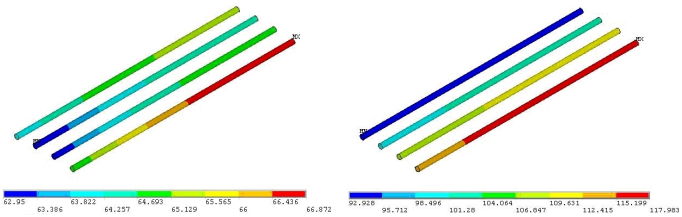

(e) Bar temperature with no load (f) Bar temperature with rated load

Fig. 4 Electromagnetic field, eddy current and temperature distributions of damper bars with no load and rated load

TABLE II
LOSSES AND TEMPERATURES OF THE DAMPER BARS WITH DIFFERENT OPERATING CONDITIONS

Operation condition	Loss (W)					Temperature (℃)	
	P_1	P_2	P_3	P_4	ΣP	T_{max}	T_{min}
No load	73	34	34	72	213	67	63
Rated load	334	231	139	84	788	118	93
Rated load with 12% negative current	397	270	182	128	977	124	98

where P_1-P_4 and ΣP are the loss of the 1th-4th damper bar and the total losses of the damper bars respectively, T_{max} and T_{min} are the maximal and minimal temperature of the damper bars respectively.

Fig. 4 and TABLE II show that the distribution of the magnetic field about the center axis of the pole is symmetric when the generator operates with no load, and the eddy current and loss of the damper bar are then basically symmetrical about the pole center axis. The losses of the 1th and 4th damper bar are roughly equal, the losses of the 2th and 3th damper bar are roughly equal too. Because of the armature reaction, the distribution of the airgap magnetic field is distorted when the generator operates with rated load. The magnetic field on the windward is weakened while it is strengthened on the lee side. The symmetry of the eddy current and loss distribution of the damper bars will no longer exist. The eddy current and loss of the 1th damper bar are significantly larger than those of the 4th damper bar. The temperature of the damper bars located near the lee side is higher than that of located near the windward. The maximal temperature occurs at the axis middle of the 1th damper bar and the minimal temperature occurs at the end of the 4th damper bar. The loss and the temperature of the damper bars increase obviously when the operating conditions of the generator change from no load to symmetric rated load and then to asymmetric rated load with 12% negative sequence current. The loss and temperature of the damper bars for 12% negative sequence current are maximal respectively. The maximal temperature with this condition is 1.85 times higher than that with no load, that is to say the temperature increases 57 ℃. The results show that the operating conditions influence the loss and heat of the damper bars obviously. In the following discussions, the operating condition of asymmetric rated load with 12% negative sequence current will be focused.

B. *The influence of damper bar pitch*

Losses and temperatures of the damper bars for 6 different damper bar pitch with 12% negative sequence current load are listed in TABLE III, in which t_1 is the stator slot pitch and keeps unchanged, t_2 is the damper bar pitch. The results show that the losses and temperatures of damper bars increase obviously with the decrease of t_2. Because of the uneven airgap of the generator, when t_2 decreases, each damper bar gets closer to the center axis of the pole and larger eddy current is induced. Therefore, the losses and temperatures of the damper bars also increase. When t_2/t_1 decreases from 0.93 to 0.7, the maximal temperature of the damper bar increases from 124 ℃ to 170 ℃ and the temperature rise is 46 ℃.

Design data t_2/t_1 of the generators at *Tongzihao*, *Linjintan* and *Feilaixia* hydropower stations are 0.93, 0.59 and 0.9 respectively. It is easy to find that the design of *Tongzihao* hydro-generator is more reasonable for avoiding over heat. In the following discussions, keep $t_2/t_1 = 0.93$ constant.

C. *The influence of damper bar assembling airgap*

The air gap between the damper bar and the damper slot is called assembling airgap in this paper and is symbolized as δ_B. Temperatures of the damper bars for 3 different δ_B with 12% negative sequence current load are listed in TABLE IV.

Because δ_B is very small and has few influence on the electromagnetic field, the losses of the damper bars for different δ_B are basically the same and then not be tabled. On the other hand, with the increase of δ_B, the heat conductivity of the assembling airgap becomes poorer and the temperature of the damper bars becomes higher. To control the temperature rise of the damper bars, it is necessary to limit δ_B. Design data δ_B of the generators at *Tongzihao*, *Linjintan* and *Feilaixia* hydropower stations are 0.15mm, 0.5mm and 0.4mm respectively. The design of *Tongzihao* hydro-generator is more reasonable for avoiding over heat.

D. *The influence of airgap length*

Keeping the stator slot width b_s unchanged and reducing the airgap length δ, more computations are carried out. Losses and temperatures of the damper bars for 3 different δ with 12% negative sequence current load are listed in TABLE V.

With the decrease of δ, the airgap flux density and the stator tooth harmonics increase. These factors lead to the increase of the loss and temperature of the damper bars. Design data b_s/δ of the generators at *Tongzihao*, *Linjintan* and *Feilaixia* hydropower stations are 3.4, 3.2 and 2.9 respectively. However, the uneven airgap length is used on *Tongzihao* generator and the equivalent b_s/δ is 2.7 when uniform airgap is referred.

TABLE III
LOSSES AND TEMPERATURES OF THE DAMPER BARS FOR DIFFERENT PITCH

t_2/t_1	Loss (W)					Temperature (℃)	
	P_1	P_2	P_3	P_4	ΣP	T_{max}	T_{min}
0.93	397	270	182	128	977	124	98
0.90	413	290	218	152	1073	127	100
0.85	502	360	290	179	1331	136	105
0.80	583	478	373	190	1624	144	107
0.75	626	632	458	162	1878	156	111
0.70	633	790	513	144	2079	170	112

TABLE IV
TEMPERATURES OF DAMPER BARS FOR DIFFERENT δ_B

δ_B (mm)	T_{max} (℃)	T_{min} (℃)
0	101.42	89.64
0.15	124.42	97.56
0.25	138.58	102.08

TABLE V
LOSSES AND TEMPERATURES OF THE DAMPER BARS FOR DIFFERENT AIRGAP

b_s/δ	Loss (W)					Temperature (℃)	
	P_1	P_2	P_3	P_4	ΣP	T_{max}	T_{min}
2.5	239	145	124	97	605	109	93
3.4	397	270	182	128	977	124	98
4.0	486	325	221	136	1168	129	98

E. The influence of damper bar diameter

To discuss the influence of damper bar diameter d_B, losses and temperatures of 3 different d_B with 12% negative sequence current load are listed in TABLE VI.

With the decrease of d_B, the total losses of the damper bars remain almost unchanged. However, the loss density, heat resistance of the assembling airgap and then the temperature of the damper bars increase due to the decrease of d_B. To prevent from the over heat and mechanical vibration of the damper bars, d_B should be enlarged appropriately. Design data d_B of the generators at *Tongzihao*, *Linjintan* and *Feilaixia* hydropower stations are 15mm, 9.5mm and 16mm respectively.

F. The influence of damper bar resistivity

To discuss the influence of conductive materials on the losses and temperatures, 3 different damper bar materials are used and their resistivities ρ_B at 120 ℃ are listed in TABLE VII. The losses and temperatures of the damper bars for 3 different ρ_B with 12% negative sequence current load are listed in TABLE VIII. The results show that the losses and temperatures of the damper bars increase with the increase of ρ_B. Good conductive materials, such as copper, are appropriate.

G. The influence of heat dissipation coefficient of field winding

Temperatures of the damper bars for 4 different heat dissipation coefficients of field winding with 12% negative sequence current load are listed in TABLE IX. The surface heat dissipation coefficients of field winding with the rectangular and septangular cross sections are 72.8 W/m^2.℃ and 101.1 W/m^2.℃ respectively. The results show that the field winding with the septangular cross section leads to a lower temperature rise of damper bars due to its larger surface area of heat dissipation.

TABLE VI
LOSSES AND TEMPERATURES OF THE DAMPER BARS FOR DIFFERENT d_B

d_B (mm)	Loss (W)					Temperature (℃)	
	P_1	P_2	P_3	P_4	ΣP	T_{max}	T_{min}
20	405	332	198	115	1049	119	97
15	397	270	182	128	977	124	98
9.5	374	248	196	191	1008	133	107

TABLE VII
RESISTIVITIES FOR DIFFERENT MATERIALS OF DAMPER BARS

Material	Copper	Alloy	Brass
resistivity ρ_B ($\times 10^{-7}$ Ω.m)	0.25	0.4	0.77

TABLE VIII
LOSSES AND TEMPERATURES OF THE DAMPER BARS FOR DIFFERENT ρ_B

Material	Loss (W)					Temperature (℃)	
	P_1	P_2	P_3	P_4	ΣP	T_{max}	T_{min}
Copper	397	270	182	128	977	124	98
Alloy	449	275	196	156	1076	128	99
Brass	534	301	247	250	1332	138	108

TABLE IX
TEMPERATURES OF THE DAMPER BARS FOR
DIFFERENT HEAT DISSIPATION COEFFICIENTS OF FIELD WINDING

Heat dissipation coefficient (W/m^2.℃)	T_{max} (℃)	T_{min} (℃)
101.1	124.42	97.56
91.0	127.46	100.61
80.9	130.93	104.12
72.8	133.93	107.82

TABLE X
TEMPERATURES OF THE DAMPER BARS FOR DIFFERENT ROTOR CORE MATERIALS

λ_r/λ_a	T_{max} (℃)		T_{min} (℃)	
	Copper bar	Brass bar	Copper bar	Brass bar
55.6/4.0	101.27	106.72	89.16	91.58
51/19.6	101.42	106.90	89.04	92.74
40.6/3.4	102.24	107.88	88.82	92.31
19/4.0	105.10	111.40	88.02	91.11
16/1.95	105.88	112.40	87.74	90.81

H. The influence of heat conductivity of iron core

Considering the anisotropic heat conductivity of the rotor core lamination, the radial and axial heat conductivities, λ_r and λ_a, are different. Temperatures of the damper bars for 5 different core materials with 12% negative sequence current load are listed in TABLE X. The results show that the heat conductivity of the rotor core lamination has almost no influence on the temperature of the damper bars. Even though λ_r/λ_a changes several times, the temperature of the damper bars just changes slightly due to the skin effect of heat resource on the pole shoe.

I. Verification of the results

To verify the correctness of the models and calculations in this paper, the temperature test of the field winding is carried out at *Tongzihao* hydropower station. The environmental air temperature is 47.6 ℃ and the average temperature of field winding tested is 110 ℃ with the rated load of the generator. To compare with the test data, more temperatures of the rotor parts, including damper bar, field winding and iron core, are obtained by the compositive calculations of 2D electromagnetic field and 3D temperature field. The calculated average temperature of field winding is 116.6 ℃ and is well agreed with the test dada. The relative error between the calculation and the test is less than 6%.

IV. CONCLUSION

Compared with the traditional analytical model and steady magnetic field FE model, The models proposed in this paper are more reasonable and can obtain more accurate results by compositive calculations of 2D time-varying electromagnetic field and 3D anisotropic steady temperature field.

The loss and heat distributions of the damper bars in one pole are uneven with the rated load or asymmetric load. The loss and temperature of the damper bars near the lee side are higher

than that of the windward.

The operating conditions and the structure design of the generator are the main factors which influence the loss and heat of damper bars. The effective methods for preventing from over heat of the damper bars are avoiding asymmetric load of the generator, enlarging the damper bar pitch, increasing the airgap and decreasing assembling airgap of the damper bar, et al.

The designed 36MW tubular hydro-generator has been operating safely all the times at *Tongzihao* hydropower station since July 2003. The good operating experience, as well as the good agreement between the computation and the test, show that the computing models and design results of this paper are correct.

REFERENCES

[1] Chao-Yang Li, "The Application of Bulb-type Hydro-Generator Set at Low Head Hydropower Station," *Developing*, no. 9, pp. 145-146, 2006.

[2] Jing-Bin Guo, "Analysis of Damaged Damping Winding and Magnetic Pole in Bulb Type Generator," *Chinese Power*, vol. 34, no. 7, pp. 63-67, May 2001.

[3] Dong Deng, Yu-Tian Sun, Guo-Wei Tan, Jin-Xiang Li, and Zhi-Hua An, "Analysis on Operating Faults of Generator in Feilaixia Hydropower Station," *Large Electric Machine and Hydraulic Turbine*, no. 6, pp. 13-17, 2003.

[4] A. F. Armor, and M. V. K. Chari, "Heat Flow in the Stator Core of Large Turbine Generators by the Method of Three-Dimensional Finite Elements," *IEEE Trans. on PAS.*, vol. 95, no. 5, pp. 1648-1668, September 1976.

[5] A. F. Armor, "Transient, Three-Dimensional, Finite-Element Analysis of Heat Flow in Turbine-Generator Rotors," *IEEE Trans. on PAS.*, vol. 99, no. 3, pp. 934-946, June 1980.

[6] G. K. M. Khan, G. W. Buckley, R. B. Bennett, and N. Brooks, "An Integrated Approach for the Calculation of Losses and Temperatures in the End-Region of Large Turbine Generators," *IEEE Trans. on Energy Conversion*, vol. 5, no. 1, pp. 183-194, March 1990.

[7] Wei-Li Li, Feng Zhou, Yun-Peng Hou, and Shu-Kang Cheng, "Calculation of Rotor Temperature Field for Hydro-generator as well as the Analysis on Relevant Factors," *Proceedings of the Chinese Society for Electrical Engineering*, vol. 22, no. 10, pp. 85-90, October 2002.

[8] Jia-Bin Wen , Da-Wei Meng, and Chang-Bin Lu, "Synthetic Calculation for the Ventilation and Heating of Large Water Wheel Generator," *Proceedings of the Chinese Society for Electrical Engineering*, vol. 20, no. 11, pp. 6-9, November 2000.

[9] Jia-Bin Wen, Da-Wei Meng, Mei-Lan Zhou, and Chang-Bin Lu, "Field Model Research of Ventilation and Heat and Optimal Calculation of Ventilation Structure for Large Water Wheel Generator," *Transactions of China Electrotechnical Society*, vol. 15, no. 6, pp. 1-4+64, December 2000.

[10] Ri-Shan Nan, Dong Zhang, and Wei-Li Li, "Coupled Numerical Calculation of Wave Shape Eigen Coefficient of Air-Gap Magnetic Field and Rotor Temperature Field of a Salient Pole Synchronous Generator," *Large Electric Machine and Hydraulic Turbine*, no. 4, pp. 23-26, 2003.

[11] H. C. Karmaker, "Broken Damper Bar Detection Studies Using Flux Probe Measurements and Time-Stepping Finite Element Analysis for Salient-Pole Synchronous Machines," *Symposium on Diagnostics for Electric Machines, Power Electronics and Drives*, pp. 193-197, August 2003.

[12] Deng-Jun Yan, Rui-Fang Liu, Min-Qiang Hu, and Jing-Dong Han, "A New Method to Deal With the Motion Problem in Electromagnetic Field Finite element Analysis," *Proceedings of the Chinese Society for Electrical Engineering*, vol. 23, no. 8, pp. 163-167, August 2003.

[13] Min-Qiang Hu, and Xue-Liang Huang, *Numerical Computation Method and its Application of Electric Machine Performance*, Nanjing: Southeast University Press, 2003.

[14] Yan-Nian Bai, *Design and Calculation of Hydro-Generator*, Beijing: China Machine Press, 1982.

[15] Yong-Tian Wei，Da-Wei Meng, and Jia-Bin Wen, *Heat Exchange in Electrical Machine*, Beijing: China Machine Press, 1998.